JOURNAL PRE-PROOF

This is an early version of the article, published prior to copyediting, typesetting, and editorial correction. The manuscript has been accepted for publication and is now available online to ensure early dissemination, author visibility, and citation tracking prior to the formal issue publication.

It has not undergone final language verification, formatting, or technical editing by the journal's editorial team. Content is subject to change in the final Version of Record.

To differentiate this version, it is marked as "PRE-PROOF PUBLICATION" and should be cited with the provided DOI. A visible watermark on each page indicates its preliminary status.

The final version will appear in a regular issue of *Engineering Transactions*, with final metadata, layout, and pagination.

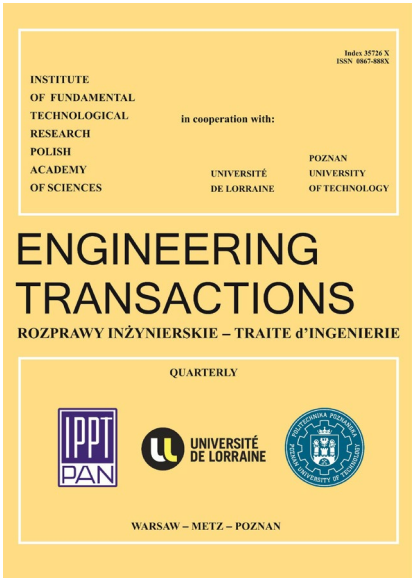

Title: Modeling Defect Detection in 3D-Printed Structures Using Ultrasonic Guided Waves

Author(s): Ismaine Zitouni, Hassan Rhimini, Abdelkerim Chouaf

DOI: https://doi.org/10.24423/engtrans.2026.3596

Journal: *Engineering Transactions*

ISSN: 0867-888X, e-ISSN: 2450-8071

Publication status: In press

Received: 2025-06-26

Revised: 2026-01-12

Accepted: 2026-01-15

Published pre-proof: 2026-01-26

Please cite this article as:

Zitouni I., Rhimini H., Chouaf A., Modeling Defect Detection in 3D-Printed Structures Using Ultrasonic Guided Waves, *Engineering Transactions*, 2026, https://doi.org/10.24423/engtrans.2026.3596

Modeling Defect Detection in 3D-Printed Structures Using Ultrasonic Guided Waves

Ismaine Zitouni [1]*https://orcid.org/0000-0002-3538-2761, Hassan Rhimini[2], Abdelkerim Chouaf[2]

[1] Interdisciplinary Laboratory of Fundamental and Applied Sciences,
Ecole Normale Supérieure, Hassan II University of Casablanca, Casablanca, Morocco

[2] Laboratory of Mechanics, Engineering And Innovation, National High School of Electricity and Mechanics, Hassan II University of Casablanca, Casablanca, Morocco

* Corresponding Author: ismaine.zitouni.doc20@ensem.ac.ma

Carbon fiber-reinforced thermoplastic composites are widely utilized in 3D printing via the fused filament fabrication (FFF) process. However, defects within printed components can compromise their performance. This study investigates the application of ultrasonic non-destructive testing (NDT) techniques for structures manufactured through FFF. Common printing defects, such as weak interlayer bonding, surface imperfections, and internal cracks, are simulated using a finite element (FE) model. The model analyzes how guided ultrasonic waves interact with these defects. The proposed methodology incorporates digital transducer control and evaluates the energy distribution across incident, reflected, and transmitted wave modes. Three representative defect types are modeled, and the approach is applied to two structural geometries: plates and pipes. The study investigates the correlation between defect size and the behavior of energy reflection and transmission. A signal processing approach is applied, using transducers positioned symmetrically along the wave propagation axis to detect mode conversion and analyze wave reflections and transmissions. The phenomenon of mode conversion is analyzed in detail, and the results are validated by ensuring energy balance consistency.

Keywords: ultrasonic, finite element simulation, guided wave, defect detection, non-destructive testing.

1. Introduction

In recent years, 3D printing has undergone significant advancements across nearly all industrial branches, particularly in car manufacturing, aerospace, and healthcare domains. These industries have seen rapid growth and diversification in printing technologies. The various techniques employed differ based on the material used, the complexity of the part being

printed, and considerations such as production and maintenance costs. For instance, methods like Selective Laser Melting (SLM) **[1]** and Selective Laser Sintering (SLS) **[2]** are well-suited for metallic materials, while Fused Deposition Modeling (FDM) **[3]** is commonly used for polymer filament printing. Despite these advances, numerous defects can still arise in printed components, stemming from a variety of causes. For exemple, defects can arise from materials themselves, for instance low interfacial bonding between fibers and the matrix in composite structures **[4,5]**. The fabrication process might also cause complications like volumetric defects, porosities, cracks, and surface pitting **[6]**. Additionally, thermal effects during production can lead to problems, such as the formation of a Thermally Affected Zone (TAZ) **[7]** notably in metal additive manufacturing processes where welding occurs. Given these potential defects, it is crucial to monitor and assess the integrity of such structures. Ultrasonic Guided Waves (UGW) **[8,9]** present a promising method for Non-Destructive Testing (NDT) of these types of structures. They are highly effective for propagating over long distances with minimal attenuation, making them ideal for assessing the structural integrity of components. To perform accurate Non-Destructive Testing (NDT) using UGW, it is essential to understand the wave dispersion characteristics. The transducer must generate frequencies corresponding to specific modes indicated by the dispersion curves. Ultrasonic sensors are then used to measure the normal displacements on the surface of the structure being tested. Post-processing techniques, such as signal analysis using Fourier transform, wavelets or other methods are essential for detecting and characterizing potential defects within a structure. Certain researchers developed numerical models to simulate the propagation of UGW in various structures. For example, A. De Luca **[10]** utilized a finite element model in ABAQUS to study UGW propagation in a Carbon Fiber Reinforced Polymer (CFRP) laminated plate, analyzing how defect size and orientation impact structural integrity. Chui *et al*. **[11]** focused on delamination detection in a 3D laminate composed of four composite layers. H. Rhimini *et al*. **[9]** explored the interaction of UGW with an embedded volumetric defect in a three-layer aluminum/epoxy/aluminum assembly, also using ABAQUS. In that study, post-processing involved applying a double Fourier transform to the data. In recent years, several researchers have started investigating the detection of defects in 3D-printed parts using ultrasound. Among them, Sarah K. Everton *et al*. **[12]** focused on identifying sub-surface defects through laser-generated ultrasound. Ian Cummings *et al*. **[13]** developed an in-situ method to detect defects as they arise in plastic parts produced by the FDM process, though post-processing the data still presents significant challenges. Caminero *et al*. **[14]** employed ultrasound with the phased array technique to assess damage in laminated 3D-printed composites. Despite these efforts, the use of ultrasonic guided

waves for defect detection remains underexplored, and post-processing techniques for interpreting the results continue to be a major hurdle.

In this study, we aim to carry out a numerical non-destructive inspection of Carbon Fiber Reinforced Thermo-Plastic (CFRTP) composite parts using guided waves **[15]**. CFRTP composites are widely used in filament manufacturing processes due to their superior mechanical properties compared to pure thermoplastics **[16,17]**. Additionally, the high prototyping flexibility and various printing parameters specific to the FDM process, such as raster angle and filament size, enable the fabrication of complex structures with CFRTP, making it a popular choice in industries like car manufacturing and aerospace. Nevertheless, the rigidity of printed CFRTP composites can degrade due to imperfections such as ruptures, layer detachment, and notches, often caused by printing parameters **[18,19]**.

In our analysis, the parts considered exhibit rectangular notches and cracks. To inspect these structures, we first generated dispersion curves for the material, representing the (frequency, wavenumber) pairs that could excite ultrasonic guided waves (UGW) in our waveguide **[20,21]**. Additionally, we plotted normalized displacement profiles with energy flow across the section, applying a spatial distribution of displacements over 10 cycles, using a Hanning window centered on the excitation frequency for weighting.

Based on these elements, we developed a numerical finite element simulation of the ultrasonic guided wave implementation process in composite plates and cylindrical pipes. We also simulated the collection of signals both before and after encountering a defect using finite element software. By calculating reflection and transmission coefficients, we analyzed how defect size and position affect the selection of the appropriate ultrasonic mode for inspection. As the defect size increases, the reflected wave packet also grows larger. Moreover, when the defect is asymmetrically positioned with respect to the median plane in the plates, mode conversion occurs, a phenomenon we addressed using a technique based on summing and subtracting the signals captured by the ultrasonic transducers.

2. Theory of ultrasonic guided waves

2.1. Dispersion network

We analyze the spread of UGW through a composite waveguide. The material in question is a carbon fiber-reinforced thermoplastic commonly used in 3D printing particularly through the FDM process. UGWs enable comprehensive scanning of the entire waveguide structure. However, to achieve this, it is essential to understand the dispersion patterns of these waves. Since UGWs are highly frequency-dependent, even a small frequency change can significantly

alter wave behavior. These dispersion patterns, known as dispersion curves, help identify the frequency f and wave number k pairs that can generate UGWs within the composite waveguide. Various methods have been applied to characterize this dispersive nature. There are approaches that include analytical techniques to find the zeros of a function **[22]**, as well as numerical techniques to plot these curves **[23]**. In our study, we implemented a MATLAB program that uses a numerical spectral method **[22]** to plot dispersion patterns for composite materials. The method applies a spectral scheme to approximate the differential equations of the governing motion and edge conditions. By determining the eigenvalues (frequencies) for a specified range of wavenumbers, and using a vibrational state-based mode separation algorithm, we obtain the dispersion curves in terms of frequency and wavenumber. Additionally, we can represent these curves in other formats, such as phase velocity V_p versus frequency or group velocity V_g versus frequency, which provide insights into the energy transport of the wave packet.

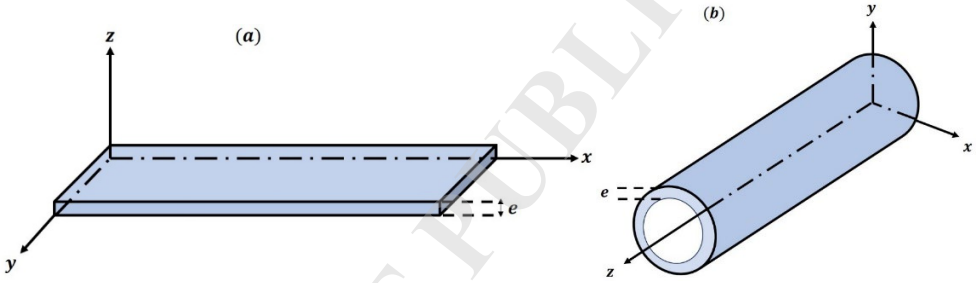

Fig. 1. Planar waveguide (a); cylindrical waveguide (b); (x,y,z)-Cartesian coordinate; *e*-thickness of the waveguide.

We consider two waveguides. The first is a 4 mm thick CFRTP composite plate (Fig. 1a) and the second is a CFRTP composite pipeline with an inner radius of 50 mm and an outer radius of 56 mm (Fig. 1b). The values of the components of the elastic stiffness tensor and the density of the composite are shown in Table 1. We note that the value of the constants are obtained in the Cartesian basis.

Table 1. Characteristics of CFRTP composite **[4].**

Density [g/cm^3]	$C'_{11}= C'_{22}= C'_{33}$	$C'_{12}= C'_{13}$	$C'_{55}= C'_{66}$	C'_{44}	C'_{23}
1,6	43.3294	6.4745	9.51	18.4291	6.4712

Figure 2a presents the dispersion curves for the CFRTP composite plate in a (product of the frequency and thickness, phase velocity) plane. The plate exhibits Lamb modes, including symmetric modes (S_n) and antisymmetric modes (A_n) with respect to the propagation planes. The fundamental modes, denoted as S_0 and A_0, are commonly used in ultrasonic guided wave (UGW) non-destructive testing **[24,25]**. Figure 3 illustrates the vibrational states (Von Mises stress) of the plate under these modes. We can see that the symmetrical S_n mode is symmetrical with respect to the u_x displacement (displacement in the direction of propagation x) and antisymmetric with respect to the u_y displacement (displacement normal to the direction of propagation). The opposite character is observed for the antisymmetric mode A_n.

Figure 2b shows the dispersion curves for a CFRTP composite cylindrical pipe. Due to the pipe's curvature, the symmetry in vibration is lost **[26]** resulting in longitudinal modes L(0,n) and torsional modes T(0,n). Additional modes, such as flexural modes F(m,n), are also present, though these are excluded from our study. The vibrational states of the pipe under the various modes are displayed in Fig. 4.

Here, n represents the mode's index, determined by its appearance at low frequencies, and m represents the order of the flexural modes.

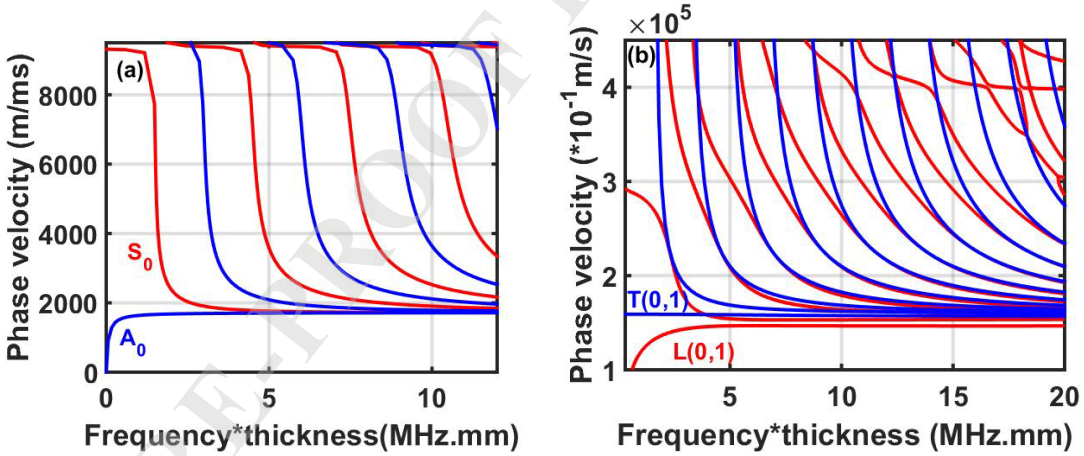

Fig. 2. Dispersion curves generated using the spectral method for a CFRTP composite in the plate of 4 mm thickness (a) and a cylindrical pipe of inner radius 50 mm and outer radius 56 mm (b).

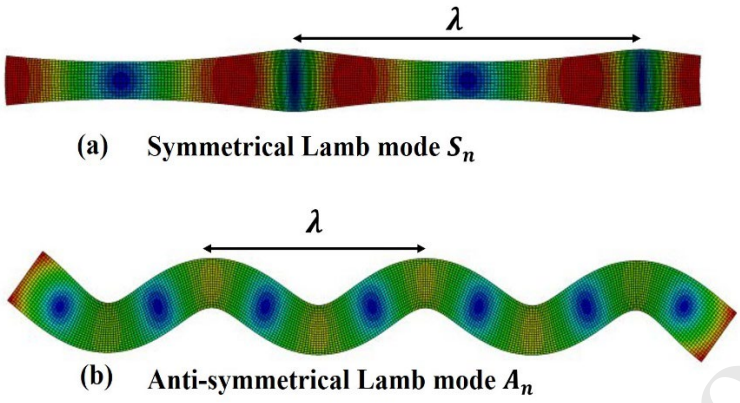

Fig. 3. Vibrational states of the plate: (a) symmetrical mode and (b) antisymmetrical mode. λ represent the wavelength.

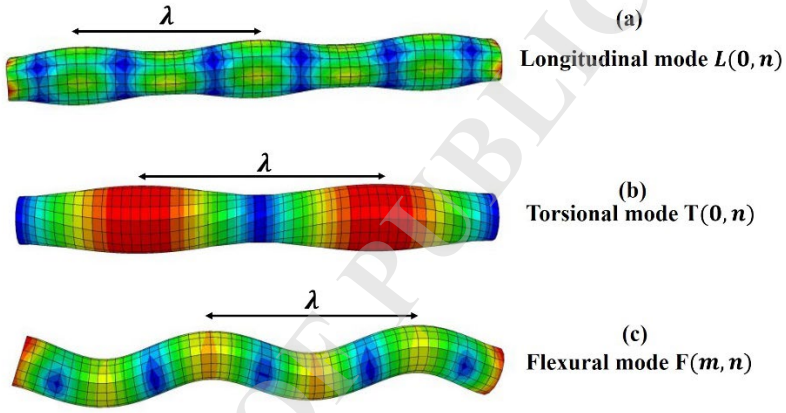

Fig. 4. Vibrational states of the cylindrical pipe: (a) longitudinal mode, (b) torsional mode and (c) flexural mode. λ represent the wavelength.

2.2. Field of displacement

Nayfeh *et al*. **[27]** have proposed the expression of displacement fields that describe the propagation of a harmonic wave in plane and cylindrical structures that are homogenous and anisotropic in shape:

$$\begin{cases} (u_x, u_y, u_z) = \sum_{q=1}^{6} (1, V_q, W_q)\, U_{1q}\, e^{ik(x+\alpha_q z - ct)} \\ (u_r, u_\theta, u_z) = U_\beta^{mn}(r)\Theta_\beta^{mn}(m\theta) e^{i(\omega t - k^{mn} z)} \end{cases}, \tag{1}$$

where q is the summation index, x is the UGW propagation direction, c is the wave phase velocity, k is the wavenumber and U_{1q},V_q, W_q are the displacement amplitudes **[27],** α_q is the ratio of the wavenumbers in the x and z directions, U_β^{mn} and the sinusoidal function Θ_β^{mn} are the radial and circumferential components of velocity.

3.Numerical simulation

3.1. Formulation

We employ the Finite Element Method (FEM), where the structure is discretized into finite elements. Within each element, the displacement field is approximated using interpolation functions at each node, resulting in what are known as nodal displacements. The global equation system is then constructed by assembling these individual element displacements. For the non-damped case the system is expressed as follows:

$$[M]\{\ddot{U}\}+[K]\{U\}=\{F\}, \tag{2}$$

where [M] represent the global mass matrix, [K] is the global stiffness matrix, {U} is the global displacement vector, $\{\ddot{U}\}$ is the global acceleration vector and {F} is the global charge vector.

In order resolve the Eq. (2), we apply Newmark's method **[28]** to approximate the spatial partial derivatives. By utilizing extended mean value theorem, Newmark's method provides an approach to solve the first time derivative as follows:

$$\{\dot{U}_{t+\Delta t}\}=\{\dot{U}_t\}+\Delta t\{\ddot{U}_\gamma\} \tag{3}$$

with

$$\{\ddot{U}_\gamma\}=(1-\gamma)\{\ddot{U}_t\}+\gamma\{\ddot{U}_{t+\Delta t}\} \tag{4}$$

Since we have partial derivatives with respect to time in the acceleration vector, the theorem can also be written as:

$$\{U_{t+\Delta t}\}=\{U_t\}+\Delta t\{\dot{U}_t\}+\Delta t^2((1-\beta)\{\ddot{U}_t\}+\beta\{\ddot{U}_{t+\Delta t}\}) \tag{5}$$

with γ and β are integration factors of Newmark. Δt is the step time.

3.2. Finite element analysis model

We examine the propagation of UGW in two types of CFRTP structures. The first structure is a homogeneous plate with length of L = 500 mm and thickness of e = 4 mm. The second structure is a hollow cylindrical pipe with an inner radius of 50 mm, an outer radius of 56 mm, and a length of L = 600 mm. We consider a linear, homogeneous dynamic calculation with no damping. The waveguide is initially not subjected to any stress, and the contact between the sensors and the structure is considered perfect. The small perturbations assumption is applied.

This study addresses a spatial-temporal problem, simulated in ABAQUS. Details regarding simulation parameters, including the spatial and temporal discretization steps Δx and Δy, will be provided later. To mesh our models, we select a control frequency of f = 500 kHz (based on

the dispersion curve) and use an element size of 0.5 mm, which meets the following condition **[29]**:

$$\max(\Delta x, \Delta y) \leq \frac{\lambda_{\min}}{10}, \tag{6}$$

with λ_{min} is the minimal wavelength **[29]**.

This criterion specifies that, to ensure computational convergence, the element size used to mesh the waveguide should be no larger than one-tenth of the smallest wavelength of the propagating modes in the structure.

For time discretization, ensuring convergence in ultrasonic simulations demands that the smallest wavelength within the UGW pulse needs to be divided into at least 20 nodes. Given a frequency of f = 500 kHz, we get a temporal step of 0.1 μs, adhering to the following condition **[30]**:

$$\Delta t = \frac{1}{20 f}, \tag{7}$$

with *f* is mode frequency selected to produce ultrasonic guided wave.

3.3. UGW generation

To numerically generate ultrasonic guided waves (UGWs) in the waveguide, several researchers have modeled the excitation signal as a specific point force, typically represented by a sinusoidal waveform modified by a Hanning window **[31,32]**. Other studies have employed piezoelectric transducers to generate UGW, applying a nodal load around the circumference of a circle [**32]**. Additionally, another approach has incorporated Snell-Descartes laws to calculate wave incidence angles [**32]**. Despite the advantages of these methods, using a cyclic force can lead to edge reflection issues. This problem has been addressed in two ways: either by treating the edges as absorbing (resulting in no reflection) or by applying post-processing techniques to the acquired signals. To mitigate these issues and ensure the excitation of the desired mode, Rhimini *et al*. **[9]** utilized analytical displacements through the thickness of an isotropic multilayer laminate to effectively excite the Lamb modes.

In this study, we focus on the last approach to model the propagation of ultrasonic guided waves (UGWs) in both an anisotropic plate and a cylindrical pipe. Generation based on analytical displacement, scaled by acoustic power is applied . For the plate, we will generate the antisymetrical A_0 mode according to previous research that indicates that the S_0 and A_0

modes are the most commonly utilized, as they are situated at low and high frequencies respectively. Additionally, the mode conversion phenomena associated with these modes are relatively straightforward **[24,25]** and both can be generated at low frequency values. For the cylindrical pipe, we have selected to generate the first longitudinal mode L(0,1) **[34]**.

Equation (1) report an analytical displacement that contain two parts: the first component describ spatial coordinate and the second one the time coordinate. Spatial component illustrates mode shape generated across the thickness of the waveguide. For example, the chosen A_0 mode show an antisymmectric longitudinal displacement (blue curve in Fig. 5a) and a symmetrical transverse displacement throughout the plate's thickness (red curve in Fig. 5a). Figure 5b displays the displacement profiles for the chosen longitudinal mode L(0,1).

The temporal component is represented by the exponential term, resulting in the analytical spatial displacements oscillating according to either a cosine or sine function. The displacement fields can be expressed immediately as functions of cosine or sine in isotropic materials **[27]**. However, in the case of highly anisotropic materials, such as in our study, it is not possible to definitively determine if the displacements are described by a cosine or sine pattern. To address this, during mapping spatial displacements at a particular position x and constant time t, the term in exponential is solely dependent on the z direction ($e^{i\varphi} = \cos(\varphi) + i\sin(\varphi)$). Thus, for an imaginary displacement, it corresponds to a sine function; otherwise, it corresponds to a cosine function. For the plate, the displacement u_x follows a sine function, while the displacement u_z follows a cosine function (mode A_0). The same approach is applied to the L(0,1) mode

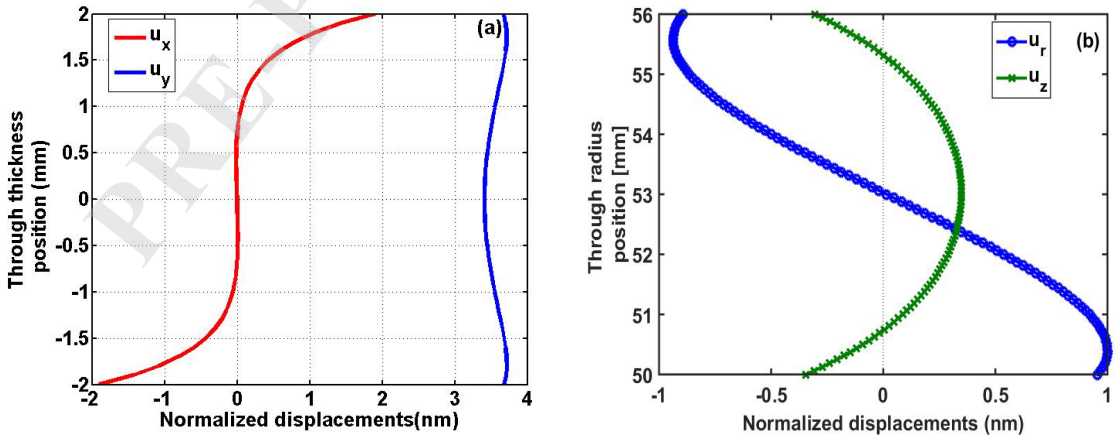

Fig. 5. Normalized analytical displacements based on the acoustic power of the selected mode A_0 of the composite plate (f=500 kHz, k=1431 m^{-1}) (a) and L(0,1) mode of the composite pipe for the couple (f=500kHz,k=67m^{-1}) (b).

The displacement's spatial distribution is used for 10 cycles, with weighting based on a Hanning window centered around the excitation frequency **[35]**. The use of Hanning window allows to exclude disturbances from the incoming signal (Fig. 6).

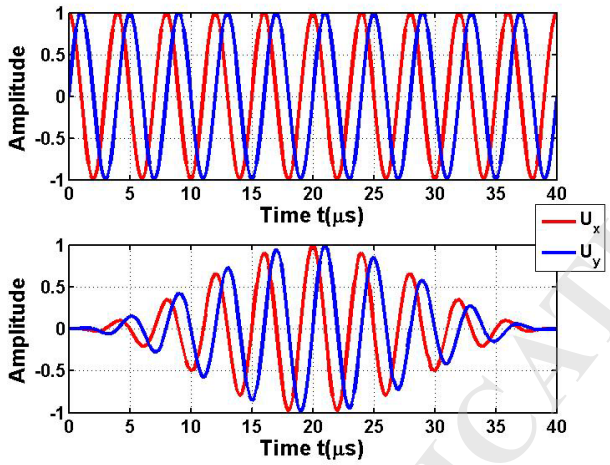

Fig. 6. Hanning window of the incident signal of the CFRTP composite plate.

3.4. Inspection of the plate

On the left side of the plate, ultrasonic guided waves are induced to travel through its thickness. Transducers are placed on the plate's surfaces y=±h to track their movement along it, ahead of and past the defect. Proper positioning of these transducers with respect to the plate edges and the defect is critical. UGWs consist of propagating modes, which are utilized in inspection, and evanescent modes **[36,37]**. With their pronounced attenuation in the material, evanescent modes are not viable for ultrasonic non-destructive testing of large-scale structures. Evanescent modes become evident when reflections occur due to the plate edges or defects. Consequently, ultrasonic sensors placed close to the defect or the edge of the structure may pick-up signals not only from the propagating modes but also from the evanescent modes. This can complicate the interpretation of results, particularly if there is insufficient information regarding the characteristics of the evanescent waves. In this study, transducers are positioned to maintain a minimum distance of at least 10 mm from both the defect and the edge. The selected transducers measure the displacements u_x and u_y at 180 nodes along the structure's interface, with the nodes spaced evenly at 0.5 mm (mesh step). In scenarios where the defect's location is unknown (as in real cases), it is essential to conduct a thorough investigation of the evanescent modes to understand and effectively address the near-field wave-defect interaction phenomena.

Temporal displacements at the plate's upper and lower surfaces, before the defect, are acquired using transducers 1 and 2. After the defect transducers 3 and 4 record temporal displacements at the plate's upper and lower surfaces (Fig. 7). Transducers 1 and 2 recorded signals that encompass two wave packets. The first one originating from incident wave and the second one is due to the reflexion of the wave. Signals collected from transducers 3 and 4 corresponds to the transmission of the wave across the defect. The arrangement places transducer 1 vertical to the position of transducer 3, as well as transducers 2 and 4. This configuration allows us to determine by assessing the time of flight between the incident and reflected waves, the defect's position, since we know in advance the phase velocity of the emitted wave. Additionally, the nature of the modes in the reflected and transmitted wave packets can be identified by examining the symmetry and anti-symmetry characteristics of the S_0 and A_0 modes. To distinguish nature of modes in reflexion and transmission, some researchers utilized tools like the double Fast Fourier transform of the recorded signals and the wavelet transform **[9,28]**.

In the initial step, the notch is assumed symmetrically located with the plate median plane. The presented configuration helps to avoid mode conversion. We first excite the A_0 mode, the wave reaches the defect. Energy from this mode is partly reflected and partly transmitted, with the A_0 mode's nature preserved throughout. Subsequently, an asymmetric positioning of the notch relative to the plate median plane is considered. In this scenario, as the mode interacts with the defect, the reflected and transmitted wave packets will include energy contributions from both the incident mode and the converted mode due to mode conversion phenomena. We will therefore focus on assessing the influence of the notch's dimensions and position on mode conversion and energy distribution.

Initially, we manipulate the defect parameters (length p and height w) and compute the energetic coefficients of the reflection and transmition. Accuracy of the calculations presented is monitored through energy balance. Equations (8) and (9) report the formulas of the energetic coefficients:

$$R = \frac{\phi_r}{\phi_i}, \tag{8}$$

$$T = \frac{\phi_t}{\phi_i}, \tag{9}$$

where ϕ_r, ϕ_t, and ϕ_i are the reflected, transmitted and incident energy flows.

Table 2. Energy coefficients describing the interaction of the first two fundamental modes of the composite plate A_0 and S_0 modes with several dimensions of the defect.

Selected modes	Defect parameters (p=Length, w=height)	Reflection coefficient R	Transmission coefficient T	Energy Conservation R+T	Error (%)
Fundamental antisymmetric mode of the plate A_0 ($k=1431\ m^{-1}$, f=500 kHz)	p=2mm,w=1mm	0.095	0.9093	1.0043	0.43
	p=5mm,w=1mm	0.7845	0.2364	1.0209	2.09
	p=1mm,w=1mm	0.0076	0.9927	1.0003	0.03
	p=1mm,w=3mm	0.8956	0.1134	1.0090	0.90
Fundamental symmetric mode of the plate S_0 mode ($k=621 m^{-1}$, f=500 kHz)	p=2mm,w=1mm	0.086	0.907	0.993	0.7
	p=5mm,w=1mm	0.8502	0.1672	1.0174	1.74
	p=1mm,w=1mm	0.0023	0.9966	0.9989	0.11
	p=1mm,w=3mm	0.8534	0.1542	1.0076	0.76

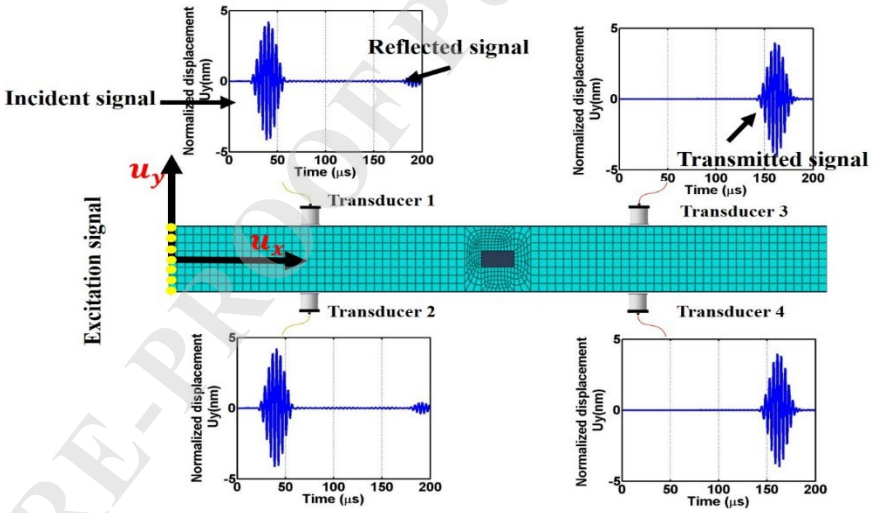

Fig. 7. Inspection of a symmetric defect on the composite CFRTP plate using the selected A_0 mode (wavenumber:k=1431 m^{-1}, frequency:f=500 kHz); lenght:p=2mm and height:w=1mm.

The reflection and transmission coefficients and the associated error are presented in Table 2. Only the A_0 and S_0 modes coexist in the plate because a frequency below the A_1 mode's cut-off frequency is chosen. Tested specimens exhibit differences in the length and height of the defect. As the defect length increases (p↑), indicating a tendency towards a longitudinal crack, the reflected energy rises, and the transmitted energy decreases, maintaining an overall energy

balance of 1. Similarly, increasing the height (w↑, transverse crack) results in a higher reflection coefficient and a lower transmission coefficient.

Figure 8 shows the scan of plate that contain asymmetrically defect position with respect to the median axis x. Two reflection signals are observed in the tranducers 1 and 2, while transducers 3 and 4 display two transmitted signals. This is due to the phenomenon of mode conversion. The A_0 mode generated initially interacts with the defect reflecting a portion of energy that depends on the defect's size. In this case, the reflected energy is split into two wave packets, a pattern also observed in the transmitted signals. To identify the type of mode reflected, several authors have applied Fourier transform or wavelet transform **[9,27]** on the captured signal, enabling a transformation from the (X, t) domain to the (k,f) domain. This (k,f) domain represents the numerically obtained dispersion curves. By comparing these with analytically derived curves, they can determine which mode has been reflected and transmitted. In this study, we propose a new method based on the symmetry of propagating modes to characterize the mode conversion phenomenon. Specifically, a symmetric mode is defined by symmetric longitudinal displacement ($u_x(+d)*u_x(-d) >0$) and antisymmetric transverse displacement ($u_y(+d) *u_y(-d) <0$), while an antisymmetric mode exhibits the opposite behavior ($u_x(+d) *u_x(-d) < 0$, $u_y(+d) *u_y(-d) > 0$) (see Figure 3). By combining the signals from transducers 1+2 and 3+4, we can remove the symmetric modes. The antisymmetric modes can be filtered out by subtracting the signals from transducers 1–2 and 3–4. Through the approach presented, the reflected captured signal contains part of the energy that corresponds to A0 mode. The other component is due to the conversion between A0 and S0 modes. A similar observation applies to the transmitted wave packet.

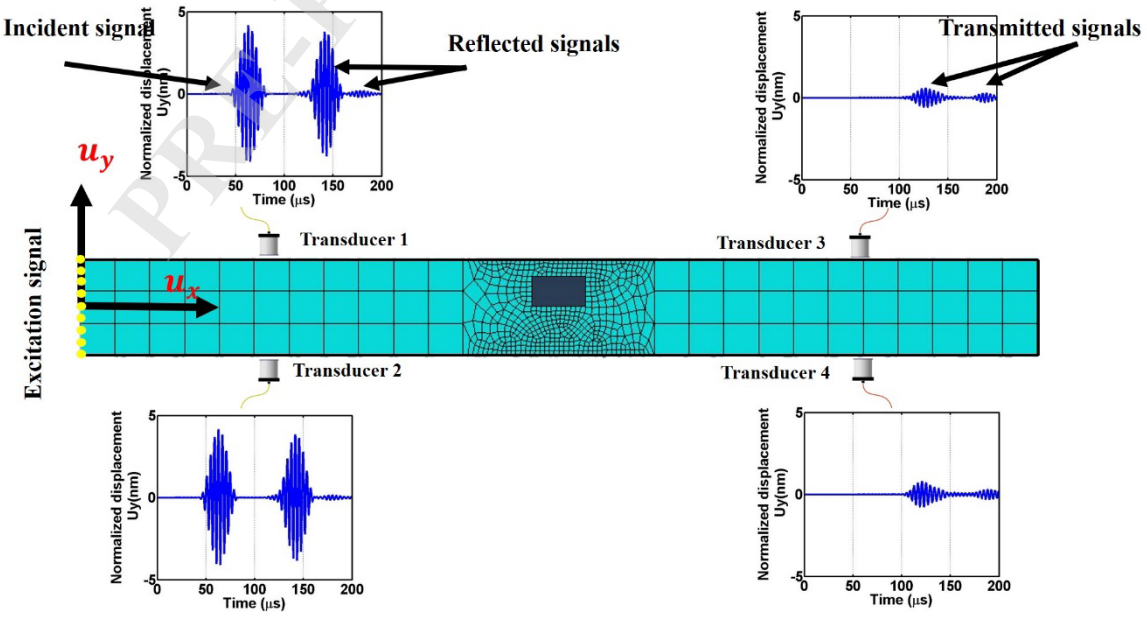

Fig. 8. Inspection of an asymmetrical defect in composite CFRTP plate using the selected A_0 mode (wavenumber:k=1431 m^{-1}, frequency:f=500 kHz); lenght:p=2mm, height:w=1.5mm.

We then calculated the energy coefficients for reflection and transmission and reported the results in table 3. Two signals are observed in the reflected wave packet due to the defect's asymmetric location relative to the propagation axis. By applying the summation and substraction technique, we determined the proportion of reflected energy that retained the original mode (A_0, R=0.8334) and that which underwent mode conversion (A_0-S_0, R=0.023). The defect's dimensions play a role in determining these values. Similar conversion results were obtained for the transmitted wave packet.

Next, we analyzed the case of an inclined defect with an inclination angle of 45° relative to the propagation axis. Figure 9 shows the scan of the composite plate with an inclined defect. In the reflection region (transducers 1 and 2), two reflected wave packets were observed, a pattern also seen in the transmission region (transducers 3 and 4). This indicates that an inclined defect induces mode conversion. To quantify the reflected and transmitted energy, we applied the summation and subtraction method (as described previously) and calculated the energy coefficients, presented in Table 4.

The results indicate a clear presence of A_0-S_0 mode conversion in both the reflected and transmitted wave packets. Additionally, the inclined defect resulted in an almost equal distribution of reflected and transmitted energy.

Table 3. Energy coefficients describing the interaction of the A_0 and S_0 modes with the defect.

Mode	Reflection coefficient R	Transmission coefficient T	Energy Conservation R+T	Error [%]
Fundamental antisymmetric mode of the plate A_0	0.310 A_0 0.227 S_0	0.309 A_0 0.183 S_0	1.029	2.9

Table 4. Energy coefficients describing the interaction of the A_0 and S_0 modes with the inclined defect.

Mode	Reflection coefficient R	Transmission coefficient T	Energy Conservation R+T	Error (%)
Fundamental antisymmetric mode of the plate A_0	0.8334 A_0 0.023 S_0	0.08 A_0 0.048 S_0	0.9764	2.32

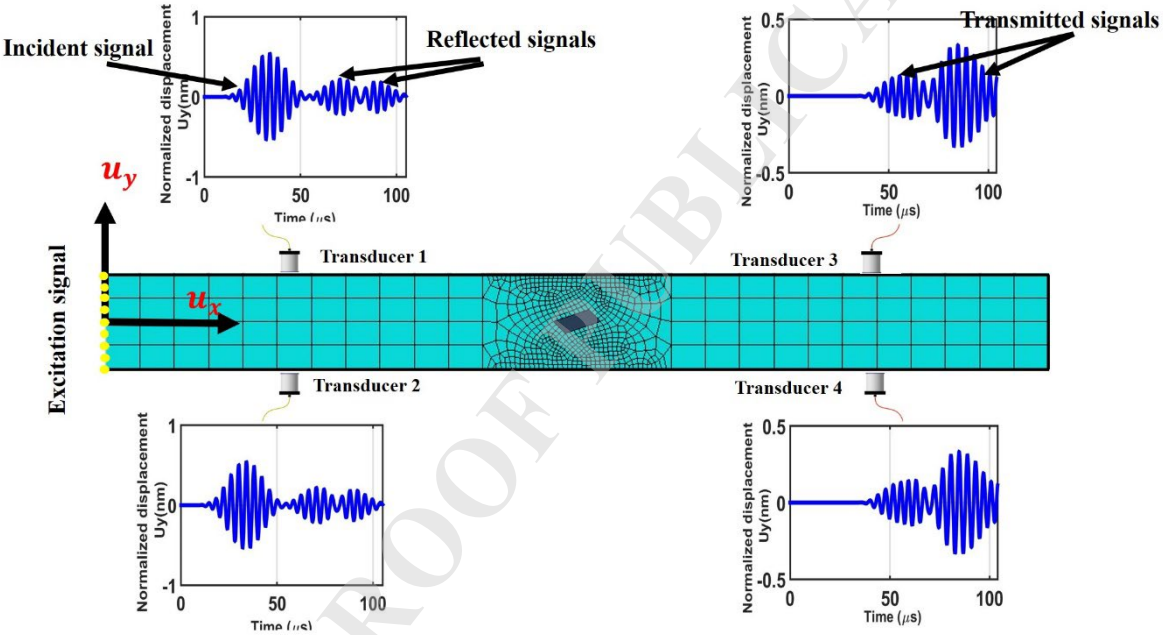

Fig. 9. Inspection of an inclined defect in composite CFRTP plate using the selected A_0 mode (wavenumber:k=1431 m^{-1}, frequency:f=500 kHz); lenght:p=2mm, height:w=1mm.

3.5. Inspection of the pipe

We now consider a cylindrical pipe with a rectangular notch defect. We generate a longitudinal mode L(0,1) along the pipe's radius. Two transducers are used: one to capture the reflected energy and the other to capture the transmitted energy. We observe two reflected and two transmitted wave packets (Fig. 10) suggests a mode conversion phenomenon **[32]**.

The cylindrical shape of the pipe disrupts mode symmetry (as shown in the dispersion curves, Fig. 2b), which prevents the use of the previous summation and subtraction method. To

address this, we analyze phase velocity to identify the modes present in the reflections and transmissions. Given the analytical phase velocity for the generated mode with f=500 kHz and k=65 m^{-1} is Vp=4688 m/s, we calculate the travel time between the incident and reflected waves **[38]**. Distance between the transducer and the defect is known, we find a numerical phase velocity of Vp=4679 m/s, corresponding to the L(0,1) mode (in close agreement with theory), and another velocity of Vp=9809 m/s, aligning with the L(0,2) mode (theoretical Vp=9817 m/s). We then compute energy coefficients for different length/height :p/w and height/length :w/p ratios, with results illustrated in Fig. 11. Figure 11(a) shows that as the p/w ratio increases (indicating a more circumferential crack), reflected energy rises while transmitted energy falls, maintaining an energy balance of 1. In Fig. 11(b), an increase in the w/p ratio (indicating a more longitudinal crack) results in a decrease in reflected energy and an increase in transmission. Thus, when the defect type is unknown, the defect's dimensional ratio and therefore its nature can be inferred from the energy coefficient trends in Fig. 11. Experimentally, in order to inspect plates and pipelines using ultrasonic guided waves, several authors use PZT transducers [39,40] (known for their light weight and ease of bonding to the surface of the waveguide without signal loss) to detect signals before and after the defect.

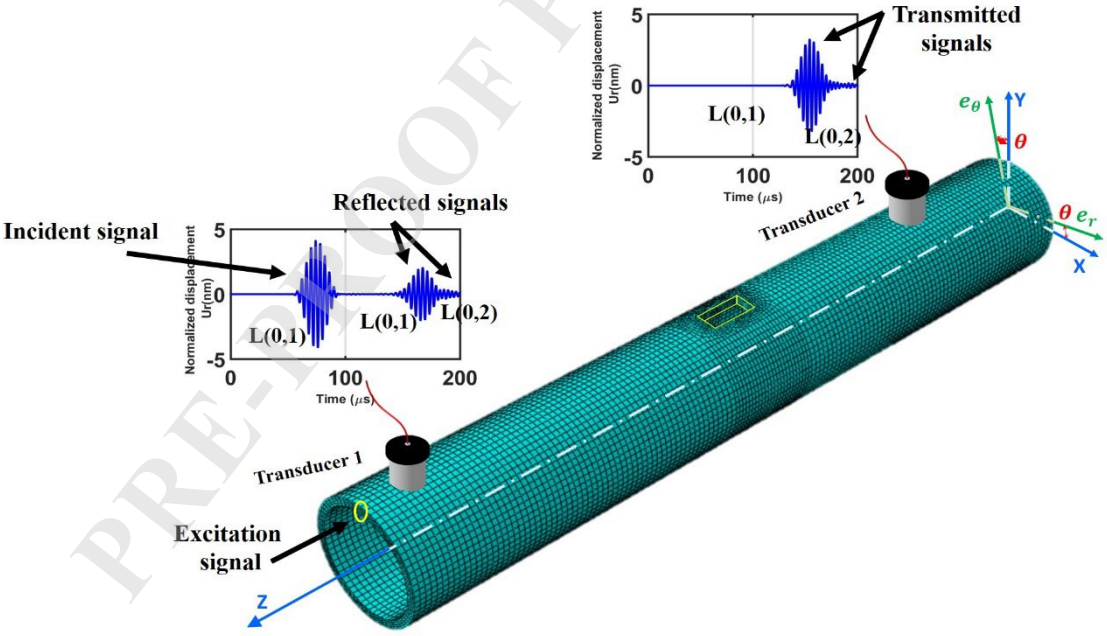

Fig. 10. Scan of the CFRTP composite cylindrical pipe using a longitudinal L(0,1) mode, (frequency:f=500kHz, wavenumber:k=67m^{-1}) with defect dimension ratio of p/w=3.

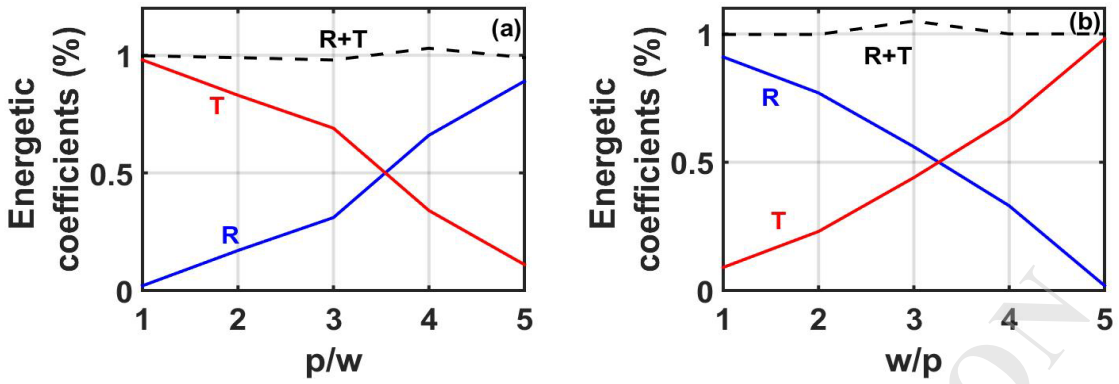

Fig. 11. Variation of energy coefficients as a function of the ratio length/height=p/w (a) and the ratio height/ length=w/p (b) ratio in the case of the pipe.

Several recent studies confirm the importance of guided-wave–based techniques for crack detection in plates and pipelines. The work of Liu *et al*. [41] stands as a major methodological reference for imaging circumferential cracks in pipes, notably through the use of full wavefield data. More recently, Silitonga *et al*. [42] provided a comprehensive review of Lamb-wave–based localization methods, detailing the conditions for selecting modes and frequencies to achieve optimal detection. Shah *et al*. [43] demonstrated through both experimental and numerical approaches, the ability of guided waves to detect the growth of internal cracks in polyethylene pipes. Zhang *et al*. [44] subsequently showed that the use of EMATs and circumferential SH modes enables the identification of defects hidden by coatings or supports, paving the way for truly non-contact inspections. Finally, Maruyama *et al*. [45] deepened the understanding of reflection and transmission phenomena at junctions of fluid-filled pipelines, highlighting the need for precise modeling to correctly interpret wave–defect interactions in complex geometries.

6. Conclusion

In this study, we simulated the propagation of UGW in composite CFRTP components produced using the FDM 3D printing technique, employing a finite element model. These structures were designed to include internal volumetric defects, such as rectangular notches and cracks, which are characteristic of FDM 3D printing. We detailed the selection of various spatial and temporal meshing parameters, and the numerical models were created by generating analytical displacements with a Hanning window weighting across the thickness of the waveguide. Strategically positioned transducers captured the reflected and transmitted signals, ensuring that only propagating waves were recorded. We implemented a novel technique involving the summing and subtracting of the captured signals to differentiate between the

various modes detected. This approach proved effective for analyzing mode conversion phenomena. The accuracy of the results was evaluated through energy balance, specifically by calculating the reflection and transmission coefficients. Our findings indicated that these energy coefficients are significantly influenced by the size of the defects. We modeled three types of defects (positioned symmetrically or asymmetrically in relation to the propagation direction, as well as inclined defects) within composite plates and cylindrical pipes. The results demonstrate the potential of guided ultrasonic waves to inspect parts with internal defects arising from the FDM 3D printing process. We also conducted a study on defect dimensions and reported novel process for determining the modal characteristics during mode conversion according to the symmetry criterion of the recorded displacements at the surfaces. Looking ahead, we seek to explore the correlation between defect parameters and mechanical properties in future work, encompassing all types of modes, including both propagating and evanescent modes.

Conflict of interest

The authors declare that they have no conflict of interest.

Funding

The authors did not receive support from any organization for the submitted work.

References

[1] Sefene E. M. (2022), State-of-the-art of selective laser melting process: A comprehensive review, *Journal of Manufacturing Systems*, **63:** 250-274, doi: 10.1016/j.jmsy.2022.04.002

[2] Gueche Y.A., Sanchez-Ballester N.M., Cailleaux S., Bataille B., Soulairol I. (2021), Selective Laser Sintering (SLS), a New Chapter in the Production of Solid Oral Forms (SOFs) by 3D Printing, *Pharmaceutics*, **13**(8): 1212, doi: 10.3390/pharmaceutics13081212

[3] Aourik O., Othmani M., Saadouki B., Abouzaid K., Chouaf A. (2021), Fracture toughness of ABS additively manufactured by FDM process, *Journal of Achievements in Materials and Manufacturing Engineering,* **109**(2), doi: 10.5604/01.3001.0015.6258

[4] Ichihara N., Ueda M., Urushiyama Y., Todoroki A., Matsuzaki R., Hirano H. (2020), Progressive damage simulation for a 3D-printed curvilinear continuous carbon fiber-reinforced thermoplastic based on continuum damage mechanics, *Advanced Composite Materials*, **29**(5): 459-474, doi: 10.1080/09243046.2020.1724430

[5] Blanco I. (2020), The use of composite materials in 3D printing, *Journal of Composites Science*, **4**(2): 42, doi: 10.3390/jcs4020042

[6] Tang C., Tan J.L., Wong C.H. (2018), A numerical investigation on the physical mechanisms of single track defects in selective laser melting, *International Journal of Heat and Mass Transfer*, **126:** 957-968, doi: 10.1016/j.ijheatmasstransfer.2018.06.073

[7] Zhang B., Li Y., Bai Q. (2017), Defect formation mechanisms in selective laser melting: a review, *Chinese Journal of Mechanical Engineering*, **30**(3): 515-527, doi: 10.1007/s10033-017-0121-5

[8] Zupančič B., Prokop Y., Nikonov A. (2021), FEM analysis of dispersive elastic waves in three-layered composite plates with high contrast properties, *Finite Elements in Analysis and Design*, **193:** 103553, doi: 10.1016/j.finel.2021.103553

[9] Rhimini H., El Allami M., Sidki M., Haddout A., Benhadou M. (2016), Ultrasonic guided waves in tri-layer structure. Application to study the interaction of guided waves with hidden defect at low frequency, *Техническая акустика*, **16:** 5,

[10] A De Luca (2016), Numerical simulation of the Lamb wave propagation in impacted CFRP laminate, *Procedia Engineering,* **167**: 109 – 115, doi: 10.1016/j.proeng.2016.11.676

[11] Chiua W.K., Roseb L.R.F., Nadarajaha N. (2017), Scattering of the fundamental anti-symmetric Lamb wave by a midplane edge delamination in a fiber-composite laminate, *Procedia Engineering,* **188**: 317 – 324, doi: 10.1016/j.proeng.2017.04.490

[12] Everton S.K., Dickens P., Tuck C., Dutton, B. (2016), Identification of sub-surface defects in parts produced by additive manufacturing, using laser generated ultrasound. *Additive Manufacturing and 3D Printing Research Group, University of Nottingham*, URL: Everton: Identification of sub-surface defects in... - Google Scholar

[13] Cummings I., Hillstrom E., Newton R., Flynn E., Wachtor A. (2016), *In-process ultrasonic inspection of additive manufactured parts. In Topics in Modal Analysis & Testing*, Volume 10: Proceedings of the 34th IMAC, A Conference and Exposition on Structural Dynamics (235-247). Springer International Publishing, doi: 10.1007/978-3-319-30249-2_20

[14] Caminero M.A., García-Moreno I., Rodríguez G.P., Chacón, J.M. (2019), Internal damage evaluation of composite structures using phased array ultrasonic technique: Impact damage assessment in CFRP and 3D printed reinforced composites, *Composites Part B: Engineering*, **165**: 131-142, doi: 10.1016/j.compositesb.2018.11.091

[15] Lee J.M., Lee C.J., Kim B.M., Ko D.C. (2020), Design of prepreg compression molding for manufacturing of CFRTP B-pillar reinforcement with equivalent mechanical properties to existing steel part, *International Journal of Precision Engineering and Manufacturing*, **21**(3): 545-556, doi: 10.1007/s12541-019-00265-z

[16] Tian X., Liu T., Yang C., *et al* .(2016), Interface and performance of 3D printed continuous carbon fiber reinforced PLA composites, *Compos Part A Appl Sci Manuf,* **88**:198–205, doi: 10.1016/j.compositesa.2016.05.032

[17] Sugiyama K., Matsuzaki R., Todoroki A. *et al*. (2018), 3D printing of composite sandwich structures using continuous carbon fiber and fiber tension, *Compos Part A*, **113**:114–121, doi: 10.1016/j.compositesa.2018.07.029

[18] Takeda N. (1995), Microscopic fatigue damage progress in CFRP cross-ply laminates, *composites,* **26**(12):859–867, doi: 10.1016/0010-4361(95)90879-5

[19] Nairn JA. (2000), Matrix microcracking in composites, *Polym Matrix Composites*, **2**(13):1–34, doi: 10.1016/B0-08-042993-9/00069-3

[20] ZITOUNI, I., RHIMINI, H., & CHOUAF, A. (2025). Comparative Study of Matrix Methods for Modeling the Dispersive Character of Ultrasonic Guided Waves. *Engineering Transactions*, *73*(2), 305-321, doi: 10.24423/engtrans.3493.2025

[21] Zitouni I., Rhimini H., Chouaf A. (2023), Modeling the propagation of ultrasonic guided waves in a composite plate by a spectral approximation method, *Engineering Transactions*, **71**(2): 213-227, doi: 10.24423/EngTrans.3073.20230510

[22] Zitouni I., Rhimini H., Chouaf A. (2024), A combined Newton–bisection approach for calculating the dispersion curves in anisotropic multilayered waveguides, *Journal of Vibration Engineering & Technologies*, **12**(3): 5189-5201, doi: 10.1007/s42417-023-01191-1

[23] Zitouni I., Rhimini H., Chouaf A. (2024), Spectral method for modeling the Dispersion of complex guided wave modes in anisotropic pipeline, *Journal of Computational Applied Mechanics*, **55**(3): 473-484, doi: 10.22059/jcamech.2024.376537.1090

[24] Benmeddour F., Grondel S., Assaad J., Moulin E. (2009), Experimental study of the A0 and S0 Lamb waves interaction with symmetrical notches, *Ultrasonics*, **49**(2): 202-205, doi: 10.1016/j.ultras.2008.08.002

[25] Wandowski T., Malinowski P., Kudela P., Ostachowicz W. (2018, March), *Analysis of S0/A0 guided wave mode conversion phenomenon*. In Health Monitoring of Structural and Biological Systems XII (Vol. 10600, 501-515), SPIE, doi: 10.1117/12.2295001

[26] Liu G., Qu J. (1998), Guided circumferential waves in a circular annulus, *Journal of Applied Mechanics*, 424-430, doi: 10.1115/1.2789071

[27] Nayfeh, A.H. (1991), The general problem of elastic wave propagation in multilayered anisotropic media, *The Journal of the Acoustical Society of America*, **89**(4): 1521-1531, doi: 10.1121/1.400988

[28] Hashamdar H., Ibrahim Z., Jameel M. (2011), Finite element analysis of nonlinear structures with Newmark method, *International Journal of the Physical Sciences*, **6**(6): 1395-1403, doi: 10.5897/IJPS11.093

[29] El Allami M., Rhimini H., Sidki M. (2015), Application of the Complex Mother Wavelet Shan 1-1.5 Processing to Lamb Modes Signals in Plates, *International Journal of Science and Research* (IJSR), **4**(1): 1849-1854 , URL: SUB15437-libre.pdf

[30] Moser F., Jacobs L.J., Qu J. (1999), Modeling elastic wave propagation in waveguides with the finite element method, *Ndt & E International*, **32**(4): 225-234, doi:10.1016/S0963-8695(98)00045-0

[31] Mohseni H.,Ng C.T. (2019), Rayleigh wave propagation and scattering characteristics at debondings in fibre-reinforced polymer-retrofitted concrete structures, *Structural Health Monitoring*, **18**(1): 303-317, doi: 10.1177/1475921718754371

[32] Pant U., Banerjee S. (2022), *Numerical modelling of ultrasonic guided waves for detection and characterisation of debonds in FRP strengthened beams*. In NDT-CE 2022-*The International Symposium on Nondestructive Testing in Civil Engineering*, doi: http://www.ndt.net/?id=27290

[33] Zheng M.F., Lu C., Chen G.Z., Men P. (2011), Modeling three-dimensional ultrasonic guided wave propagation and scattering in circular cylindrical structures using finite element approach, *Physics procedia*, **22:** 112-118, doi: 10.1016/j.phpro.2011.11.018

[34] Nayfeh, A.H. (1991), The general problem of elastic wave propagation in multilayered anisotropic media, *The Journal of the Acoustical Society of America*, **89**(4): 1521-1531, doi: 10.1121/1.400988

[35] Podder P., Khan T.Z., Khan M.H., Rahman M. M. (2014), Comparative performance analysis of hamming, hanning and blackman window, *International Journal of Computer Applications*, **96**(18), doi: 10.5120/16891-6927.

[36] Ismaine Z., Hassan R. and Abdelkerim C.(2023), *New spectral displacement post-processing approach for modeling ultrasonic guided waves*, 2023 3rd International Conference on Innovative Research in Applied Science, Engineering and Technology (IRASET), Mohammedia Morocco, 1-8, doi: 10.1109/IRASET57153.2023.10152927

[37] Ismaine, Z., Hassan, R., & Abdelkerim, C. (2025). Hybrid Spectral Approach for Ultrasonic Guided Wave Dispersion in Fluid-Loaded Anisotropic Viscoelastic Multilayered Structures. *Journal of Vibration Engineering & Technologies*, *13*(8), 1-19, doi: 10.1007/s42417-025-02120-0

[38] Väer K., Anton J., Klauson A., Eerme M., Ounapuu E., Tšukrejev P. (2017), Material characterization for laminated glass composite panel, *Journal of Achievements in Materials and Manufacturing Engineering*, **81**(1) , doi: 10.5604/01.3001.0010.2032

[39] Zhu, C., Xu, Y., Lu, H. (2025). Pipeline Unidirectional Guided Wave Generation Based on a Hybrid Piezoelectric Transducer Ring and Wave-Packet Modification. *Journal of Pipeline Science and Engineering*, 100416, doi: 10.1016/j.jpse.2025.100416

[40] Zitouni, I., Rhimini, H., & Chouaf, A. (2025). Integration of Piezoelectric Wafer Sensors PWS Signal to Generate Ultrasonic Guided Waves in Planar and Cylindrical Waveguide. *Periodica Polytechnica Mechanical Engineering*, *69*(1), 83-91, doi: 10.3311/PPme.39665

[41] Liu, K., Wu, Z., Jiang, Y., Wang, Y., Zhou, K., & Chen, Y. (2016). Guided waves based diagnostic imaging of circumferential cracks in small-diameter pipe. *Ultrasonics*, *65*, 34-42, doi: 10.1016/j.ultras.2015.10.025

[42] Silitonga, D. J., Declercq, N. F., Walaszek, H., Vu, Q. A., Saidoun, A., Samet, N., ... & Thabourey, J. (2024). A comprehensive study of non-destructive localization of structural features in metal plates using single and multimodal Lamb wave excitations. *Acta Acustica*, *8*, 66, doi: 10.1051/aacus/2024069

[43] Shah, J. K., Wang, H., & El-Hawwat, S. (2024). Detection of internal crack growth in polyethylene pipe using guided wave ultrasonic testing. *Earthquake Engineering and Engineering Vibration*, *23*(2), 319-329, doi: 10.1007/s11803-024-2238-8

[44] Zhang, X., Zhou, J., Hu, Y., Liu, Y., & Shen, X. (2024). Electromagnetic acoustic detection of pipe defects hidden above T-Type support structures with circumferential shear horizontal guided wave. *Micromachines*, *15*(4), 550, doi: 10.3390/mi15040550

[45] Maruyama, T., Matsuo, T., & Nakahata, K. (2025). Numerical study on guided-wave reflection and transmission at water pipe joint using hybrid finite element method. *Computational Mechanics*, *75*(1), 285-300, doi: 10.1007/s00466-024-02505-0